

## A novel method for preparing $\alpha$ -LiFeO<sub>2</sub> nanorods for high-performance lithium ion batteries

Youzuo Hu<sup>a,b</sup>, Xingquan Liu \*

*<sup>a</sup>R&D Center for New Energy Materials and Integrated Energy Devices, University of Electronic Science and Technology of China, Chengdu 610054, China*

*<sup>b</sup>Department of Chemistry, Lancaster University, Lancaster LA1 4YB, UK*

**Abstract:** One dimensional (1D)  $\alpha$ -LiFeO<sub>2</sub> nanorods are successfully prepared via a low temperature solid-reaction from  $\alpha$ -FeOOH nanorods synthesized by hydrothermal process and used as cathode materials in lithium ion batteries. As cathode material for lithium ion batteries, the nanorods can achieve a high initial specific capacity of 165.85 mAh/g at 0.1 C for which a high capacity retention of 81.65% can still be obtained after 50 cycles. The excellent performance and cycling stability are attributed to the unique 1D nanostructure, which facilitates the rapid electron exchange and fast lithium ion diffusion between electrolyte and cathode materials.

**Key words:**  $\alpha$ -LiFeO<sub>2</sub> nanorod; Energy storage and conversion; Nanocrystalline materials; Cathode

### 1. Introduction

Lithium ion batteries (LIBs) have been widely used as renewable energy storage devices for electronic products, plug-in hybrid and pure electric vehicles due to their high power density and stable cycling performance [1-3]. The layered  $\alpha$ -LiFeO<sub>2</sub> is considered as one of the potential candidates as cathode material for LIBs due to its high theoretical capacity (282 mAh/g), environmental friendliness and low cost [4-5]. However, there are still some challenges remained for  $\alpha$ -LiFeO<sub>2</sub> cathodes, such as inherent sluggish kinetic and poor electronic conductivity, which severely disrupts the high-rate and cycling performance of batteries [6].

Generally, the nanostructured morphology such as nanowires, nanoparticles, and nanorods can enhance their material electrochemical properties [7-9]. Among different morphologies, one dimensional (1D) nanorods have attracted numerous attentions due to their 1D transport pathway which enables good electron transport and fast lithium-ion insertion/removal [10]. However, there's still **huge challenges** to **directly** prepare  $\alpha$ -LiFeO<sub>2</sub> nanorods via conventional strategies where cubic crystals are

---

\* Corresponding authors.

*E-mail address:* lxquan@uestc.edu.cn (X. Liu).

usually obtained [11]. According to previous reports,  $\alpha$ -FeOOH nanorods have been used as a self-template to prepare 1D iron based materials, such as  $\text{Fe}_2\text{O}_3$  and  $\text{Fe}_3\text{O}_4$  [12-13]. Inspired by these, in this work, we firstly synthesize  $\alpha$ -FeOOH nanorods by hydrothermal method, then by solid-state reaction method  $\alpha$ -LiFeO<sub>2</sub> nanorods are obtained (Scheme S1). The excellent electrochemical performance of the as-prepared  $\alpha$ -LiFeO<sub>2</sub> nanorods is evaluated in LIBs and the structure-property relationship are explored based on physical characterization results.

## 2. Experimental

### 2.1. Materials synthesis

$\alpha$ -FeOOH nanorods were synthesized through a hydrothermal process. Firstly, 2.59 g  $\text{Fe}(\text{NO})_3 \cdot 9\text{H}_2\text{O}$  and 1.01 g KOH were dissolved in 80 ml distilled water, and 1 ml of  $\text{H}_2\text{O}_2$  was added to remove the  $\text{Fe}^{2+}$  in the solution. After thoroughly stirred for 1 h, the solution was transferred into a 100 ml Teflon-lined stainless steel autoclave and left at 100 °C for 6 hours.  $\alpha$ -LiFeO<sub>2</sub> nanorods were prepared via a low temperature solid-state reaction method from the as-prepared  $\alpha$ -FeOOH rods. Typically, the as-prepared  $\alpha$ -FeOOH rods were mixed with  $\text{LiOH} \cdot \text{H}_2\text{O}$  and  $\text{LiNO}_3$  ( $\text{Li}^+/\text{Fe}^{3+} = 4$ ) by grinding and then dried at room temperature. After that, the powder was sintered at 400 °C for 6 hours in muffle to obtain  $\alpha$ -LiFeO<sub>2</sub> nanorods.

### 2.2. Materials characterization

XRD analysis, materials morphologies and electronic state of each element of the sample were characterized by X-ray diffraction (XRD, Bruker DX-1000, Cu K $\alpha$  radiation), scanning electron microscopy (FESEM, JEOL, JSM-6360LV), Transmission electron microscopy (TEM) and high-resolution transmission electron microscopy (HRTEM, JEOL, JEM-3010) and X-ray photoelectron spectroscope (XPS, ESCALAB 250XI), respectively.

### 2.3. Electrochemical measurements

For battery test, the working electrode was prepared from 85% as-prepared  $\alpha$ -LiFeO<sub>2</sub> rods, 10% acetylene black, and 5% polyvinylidene fluoride. The lithium metal was used as counter electrode. The electrolyte was 1 M  $\text{LiPF}_6$  in a mixture of ethylene carbonate, dimethyl carbonate and ethylmethyl carbonate (EC: DMC: EMC, 1:1:1 by volume). The batteries were assembled in an argon filled glove box and tested on Land cell Systems (LAND CT2001A) in the voltage range of 1.5–4.8 V. Cyclic

voltammetry (CV) and electrochemical impedance spectroscopy (EIS) analysis were conducted with a CS-350 electrochemical workstation.

### 3. Results and discussion

XRD pattern of  $\alpha$ -FeOOH nanorods is shown in Fig. S1. All peaks are indexed to  $\alpha$ -FeOOH (Space group *pbnm*, JCPDS No.29-0713) [15]. XRD pattern of  $\alpha$ -LiFeO<sub>2</sub> nanorods (Fig. 1a) shows all the diffraction peaks (111), (200), (220), (311) and (222) are well regarded to the layered structure of  $\alpha$ -LiFeO<sub>2</sub> (JCPDS No. 74-2284) with lattice constants *a* = 4.158 [15-16]. No diffraction peak from  $\alpha$ -FeOOH is observed, indicating the  $\alpha$ -FeOOH nanorods is fully converted into  $\alpha$ -LiFeO<sub>2</sub> in the low temperature solid-state reaction.

The SEM image (Fig. 1b) shows the width and length of the  $\alpha$ -FeOOH nanorods are approximately 20 nm and 0.75  $\mu$ m, respectively. Fig. 1c shows the morphology of the obtained  $\alpha$ -LiFeO<sub>2</sub>, which is mainly composed of nanorods, suggesting that the rod-like morphology of the  $\alpha$ -FeOOH nanorods are remained after the solid-state reaction.

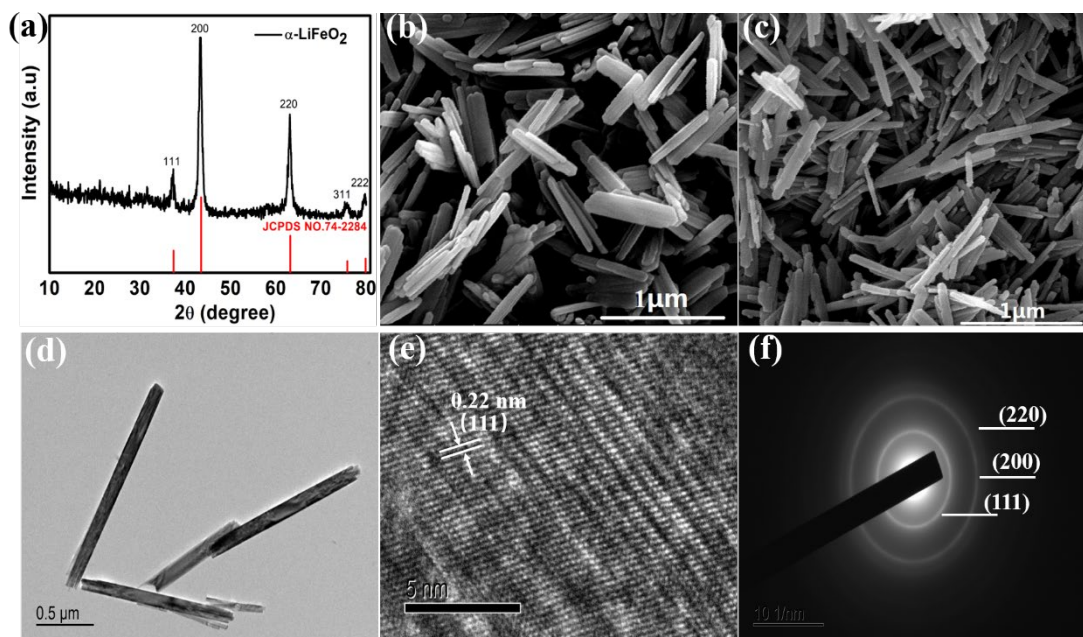


**Fig. 1.** XRD (a) pattern of the as-prepared  $\alpha$ -LiFeO<sub>2</sub>, SEM (b) image of  $\alpha$ -FeOOH, SEM (c) and TEM (d) and HRTEM (e) images with corresponding SAED pattern (f) of the as-prepared  $\alpha$ -LiFeO<sub>2</sub>.

TEM image (Fig. 1d) further confirms the diameter of  $\alpha$ -LiFeO<sub>2</sub> nanorods is around 20 nm. The HRTEM image in Fig. 1e shows the lattice fringe spacing of 0.24 nm is consistent with the (111) crystal planes of  $\alpha$ -LiFeO<sub>2</sub>. The corresponding selected area electron diffraction (SAED) pattern presented in Fig. 1e shows the diffraction rings from inside to outside as (111), (200), (220), which are in good agreement with the XRD results.

The XPS survey of the  $\alpha$ -LiFeO<sub>2</sub> nanorods (Fig. 2a) confirms that the sample comprises Li, Fe and O. The spectrum of Fe2p is depicted in Fig. 2b. The Fe2p spectrum exhibits two peaks at 711.15 eV and 724.89 eV, corresponding to Fe 2p<sub>3/2</sub> and Fe 2p<sub>1/2</sub> spin orbit peaks of  $\alpha$ -LiFeO<sub>2</sub>, respectively. Besides, both Fe 2p<sub>3/2</sub> and Fe 2p<sub>1/2</sub> main peaks show satellite peaks on their higher binding-energy sides, thus confirming the Fe (III) oxidation state [17].

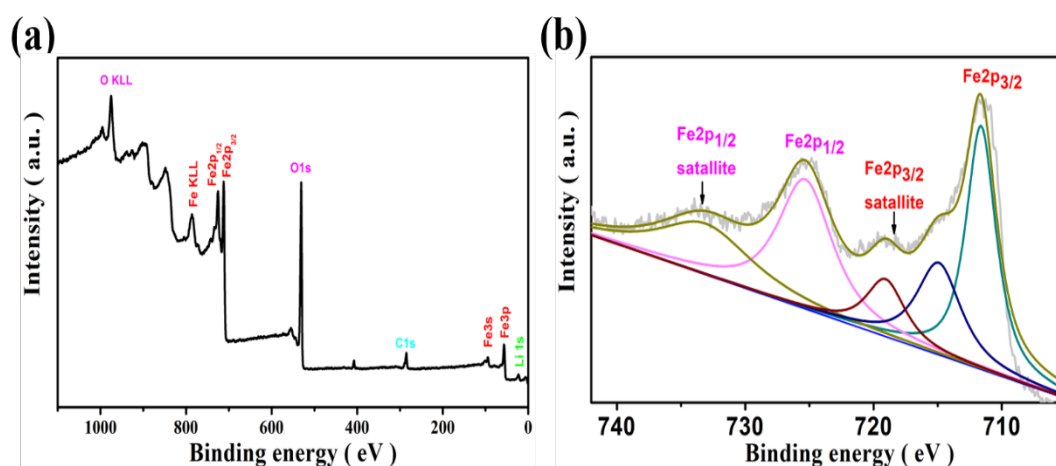


**Fig. 2.** (a) XPS survey and (b) Fe 2p spectrum of  $\alpha$ -LiFeO<sub>2</sub> nanorods.

CV, EIS and charge-discharge curves of the  $\alpha$ -LiFeO<sub>2</sub> nanorods are depicted in Fig. 3 together with its cycling performance. Fig. 3(a) shows CV curves in the voltage range of 1.5-4.8 V. The oxidation peaks appeared at 2.74 and 4.75 V are attributed to the charge process, and cathodic peaks at 1.65 V are associated with lithium insertion in the  $\alpha$ -LiFeO<sub>2</sub> nanorods [18]. Fig. 3(b) displays Nyquist plots of the  $\alpha$ -LiFeO<sub>2</sub> electrode before and after 50 cycles of cycling at 0.1 C. Both figures contain a semicircle and a diagonal line representing the charge transfer resistance ( $R_{ct}$ ) and Warburg impedance

( $\omega_0$ ), respectively [19-20].

**Table 1.** Fitting values of charge transfer resistance ( $R_{ct}$ ) and lithium ion diffusion coefficient of the  $\alpha$ -LiFeO<sub>2</sub> electrode.

	0 cycle	50 cycles
Charge transfer resistance/ $\Omega$ ( $R_{ct}$ )	151.5	183
$D_{Li^+}/\text{cm}^2 \cdot \text{S}^{-1}$	$2.7 \times 10^{-12}$	$1.5 \times 10^{-12}$

Table 1 lists the fitting value of charge transfer resistance ( $R_{ct}$ ) of  $\alpha$ -LiFeO<sub>2</sub> nanorods in batteries. The charge transfer resistance is 151.5 and 183  $\Omega$  before and after 50 cycles, respectively. The small potential difference ( $\Delta E=1.095$  V) and impedance change value ( $\Delta R_{ct}= 31.5$   $\Omega$ ) indicate that the rod-like  $\alpha$ -LiFeO<sub>2</sub> has a good electronic conductivity [21-23]. The lithium ion diffusion coefficient can be calculated using following equations [24].

$$D_{Li^+} = \frac{R^2 T^2}{2A^2 n^4 F^4 C^2 \sigma^2} \quad (1)$$

Where  $D_{Li^+}$  is the lithium ion diffusion coefficient, A is surface area of the electrode, R is gas constant, n is number of electrons, T is absolute temperature, F is Faraday constant, C is the Li-ion concentration in the electrode, and  $\sigma$  is Warburg factor shown in Fig.3c. The  $D_{Li^+}$  value of the  $\alpha$ -LiFeO<sub>2</sub> electrode is also listed in Table 1. The decrease of  $D_{Li^+}$  value after the 50 cycles is small, suggesting that one dimensional ion transport channel provided by the nanorod structure improves the Li-ion diffusion rate and enables a better rate capability of  $\alpha$ -LiFeO<sub>2</sub>.

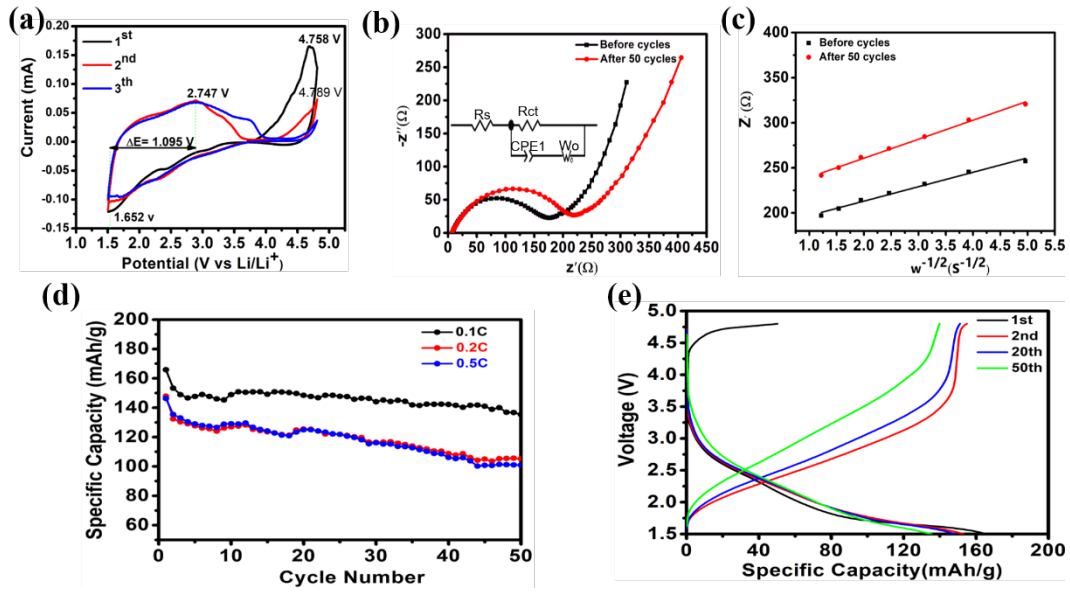


**Fig. 3.** (a) CV curves of the first three cycles, (b) Nyquist curves (the inset shows the equivalent circuit), (c) liner fitting curves of  $Z'$  vs  $\omega^{-1/2}$  and (d) cycling performance of  $\alpha$ -LiFeO<sub>2</sub> nanorods at 0.1, 0.2 and 0.5 C; (e) specific charge-discharge curves at 0.1 C of  $\alpha$ -LiFeO<sub>2</sub> nanorods

Fig. 3 (d) and (e) show cycling performance of  $\alpha$ -LiFeO<sub>2</sub> nanorod electrodes at 0.1, 0.2 and 0.5 C. The cycling performance of  $\alpha$ -LiFeO<sub>2</sub> are tested at 0.1, 0.2 and 0.5 C within the voltage range of 1.5 - 4.8 V (Fig. 3d). The initial discharge capacities of  $\alpha$ -LiFeO<sub>2</sub> are 165.85, 150.84 and 147.87 mAh/g, and these drop to 135.42, 105.23, 100.88 mAh/g after 50 cycles, respectively. Compared with  $\alpha$ -LiFeO<sub>2</sub> bulk samples reported in literature [18, 25], the  $\alpha$ -LiFeO<sub>2</sub> nanorod electrode here delivers better cycling performance at 0.2 and 0.5 C, which can be ascribed to the nanorod morphology which is beneficial for electron and lithium-ion transportation [25-26]. The charge/discharge profiles (Fig. 3e) remain nearly the same after 50 cycles, suggesting a very small polarization during cycling process.

#### 4. Conclusion

We successfully prepared  $\alpha$ -LiFeO<sub>2</sub> nanorods via a novel hydrothermal-assisted solid-state method by using  $\alpha$ -FeOOH nanorods as the self-sacrifice template. The  $\alpha$ -LiFeO<sub>2</sub> nanorod can provide one dimensional path facilitating the transportation of lithium ions. Moreover, the good electron transport property of one dimensional nanorods reduces the charge transfer impedance and thus also improves the electrode cycling performance. As a result, the  $\alpha$ -LiFeO<sub>2</sub> nanorod electrode presents a stable specific capacity of 139.8 mAh/ g<sup>-1</sup> at 0.1 C after 50 cycles, indicating the enhancement effect of the

nanorod morphology for electrochemical applications.

### Acknowledgments

This work was financially supported by the National Natural Science Foundation of China (No. 21071026) and the Outstanding Talent Introduction Project of University of Electronic Science and Technology of China (No. 08JC00303).

### Reference

- [1] G. Zubi, R. Dufo-López, M. Carvalho, G. Pasaoglu, *Renewable and Sustainable Energy Reviews*, 2018, 89:292–308.
- [2] M. Armand, J. M. Tarascon, *Nature*, 2008, 451: 652-657.
- [3] N. K. Nitta, Fei. X. Wu, J. T. Lee, G. Yushin, *Li-ion battery materials: present and future*, *Materials Today*, 2015, 18: 252-264.
- [4] J. G. Li, J. J. Li, J. Luo, L. Wang, X. M. He, *Int. J. Electrochem. Sci.*, 2011, 6: 1550-1561.
- [5] Y. Sakurai, H. Arai, S. Okada, J. Yamaki, *Journal of Power Sources*, 1997, 68: 711-715.
- [6] R. Kanno, T. Shirane, Y. Kawamoto, Y. Takeda, M. Takana, M. Ohashi, Y. Yamaguchi, *J. Electrochem. Soc*, 1996, 143: 2435-2442.
- [7] C. L. Li, N. B. Bai, H. Chen, H. Y. Lu, K. X. Xiang, *Preparation and characterization LiFePO<sub>4</sub>/C nanowires and their improved performance for lithium-ion batteries*, *Ionics*, 2015, 21:2465–2469.
- [8] F. Pignanelli, M. Romero, D. Mombrú, E. Téliz, V. Díaz, J. Castiglioni, F. Zinola, R. Faccio, Á. W. Mombrú, *Ionics*, 2019, 25:3593–3601.
- [9] L. Xue, Q. H. Zhang, X. H. Zhu, L. Gu, J. L. Yue, Q. Y. Xia, T. Xing, T. T. Chen, Y. Yao, H. Xia, *3D LiCoO<sub>2</sub> nanosheets assembled nanorod arrays via confined dissolutionrecrystallization for advanced aqueous lithium-ion batteries*, *Nano Energy* 56 (2019) 463–472.
- [10] Y. Cheng, K. Feng, Z. H. Song, H. Z. Zhang, X. F. Li, H. M. Zhang, *Nanoscale*, (2018), 10: 1997–2003.
- [11] R. Kanno, T. Shirane, Y. Inaba, Y. Kawamoto, *J. Power Sources*, 1997, 68: 145-152.

- [12] M. H. Chen, J. L. Liu, D. L. Chao, J. Wang, J. H. Yin, J.Y. Lin, H. J. Fan, Z. X. Shen, *Nano Energy*, 2014, 9: 364-372.
- [13] Y. T. Ma, J. Huang, L. Lin, Q. S. Xie, M. Y. Yan, B. H. Qu, L. S. Wang, L. Q. Mai, D. L. Peng, J. *Power Sources*, 2017, 365: 98-108.
- [14] M. Fang, M.Y. Zhu, K. Zhang, X. L. Tan, H.S. Zhu, X. K. Wang, *Mate. Lett*, 2018, 231: 76–79.
- [15] M. M. Rahman, A. M. Glushenkov, Z. Q. Chen, X. J. Dai, *Phys, Chem. Chem. Phys*, 2013, 15: 20371—20378.
- [16] C. F. Hu, Y. Y. Shang, Y. Wang, J. Xu, Y. J. Zhang, X. J. Li, A.Y. Cao, *Appl. Surf. Sci*, 2017, 405: 405–411.
- [17] Shilpa, A. Sharma, *J. Mater. Chem. A*, 2017, 5: 14220–14229.
- [18] A. E. Abdel-Ghany, A. Mauger, H. Groult, K. Zaghbi, C.M. Julien, *J. Power Sources*, 2012, 197 :285-291.
- [19] J. Morales, J. Santos-Pe, R.Trocolia, S. Frangerb, *Electrochimica Acta*, 2008, 53: 6366–6371.
- [20] Z. Y. Chen, X. Y. Yan, M. Xu, K. F. Cao, H. L. Zhu, L. J. Li, J. F. Duan, *ACS Appl. Mater. Interfaces*, 2017, 9: 30617-30625.
- [21] G. Longonia, J. K. Pandaa, L. Gagliania, R. Bresciab, L. Mannac, F. Bonaccorsoa, V. Pellegrinia, *Nano Energy*, 2018, 51: 656–667.
- [22] B. Wu, W. L. Gao, *J Mater Sci*, 2018, 53: 4433–4443.
- [23] M. Xu, Z. Y. Chen, H. L. Zhu, X. Y. Yan, L. J. Li, Q. F. Zhao, *J. Mater. Chem. A*, 2015, 3: 13933-13945.
- [24] H. Y. Zhao, S. S. Liu, X. Q. Liu, M. Tan, Z. W. Wang, Y. Cai, S. Komarneni, *Ceramics Inter*, 2016, 42: 9319–9322.
- [25] J. Morales, J. Santos-Pena, *Electrochem. Communications*, 2007, 9: 2116–2120.
- [26] M. Xu, Z. Y. Chen, L. J. Li, H. L. Zhu, Q. F. Zhao, L. Xu, N. F. Peng, L. Gong, *Journal of Power Sources*, 2015, 281: 444-454.